Phase-, Time-, and Space-Resolved Step-Scan FT-IR Spectroscopy

Principles and Applications to Dynamic and Heterogeneous Systems

Eric Y. Jiang
Thermo Nicolet

This article reviews the principles and major applications of step-scan Fourier transform–infrared spectroscopy, an important means for solving challenging problems in many areas of science and technology, including electroluminescence measurement of low-powered light-emitting devices; depth-profiling analysis of submicrometer-thick multilayered organic films; rheo-optical characterization of polymer blends; nanosecond-scale kinetics of fast chemical reactions; and chemical imaging of heterogeneity of complex samples.

The concept of step-scan mid-infrared interferometry dates back to the 1960s when the first optoelectronically controlled step-scan interferometer was reported (1). In contrast to the linear change of the optical path difference (retardation) in a conventional continuous-scan interferometer, the retardation changes stepwise in a step-scan Fourier transform–infrared (FT-IR) spectrometer. Step-scan FT-IR spectroscopy eliminates the time dependence of the interferogram and temporal Fourier frequencies created by a continuous scan. This makes step-scan FT-IR spectroscopy a very powerful tool for studying time- and phase-dependent phenomena (2). However, because of the growing acceptance of commercial continuous-scan instruments and the lack of exploration of step-scan applications, continuous-scan FT-IR spectroscopy was the only commercial product available for many years before serious commercial step-scan interferometer development took place (3–5).

Research interests in photothermal–photoacoustic IR spectroscopy and dynamic time-resolved spectroscopy in the late 1980s led to development activities of step-scan instruments both academically (6) and commercially (3). However, the use of a step-scan interferometer was initially limited to only a few research laboratories because the earlier step-scan interferometers were very sensitive to environmental vibrations and had relatively poor mirror-position control. Step-scan FT-IR spectroscopy has increased in popularity among researchers in both academia and industry since the early 1990s. The driving force behind this popularity is the extensive pioneering work performed in advanced dynamic spectroscopic applications. The commercialization of a step-scan spectrometer with a robust, digital signal processor (DSP); precise mirror-position control; and turnkey operation has made step-scan FT-IR the technical choice for a variety of applications in chemistry, physics, materials, and biomedical fields (10–12).

MODERN STEP-SCAN INTERFEROMETRY

The spectroscopic data reported in this article were collected by using either a Thermo Nicolet (Madison, WI) Nexus 870 step-scan interferometer or its predecessor, the Magna-IR 860. The Vectra-Piezo air-cushioned graphite interferometer is the heart of both the Nexus 870 and Magna-IR step-scan spectrometers. This interferometer reserves some of the key performance characteristics of an air bearing and offers many advantages for step-scan capabilities. It uses the computational power of the multiembedded digital signal processors for many interferometer functions, including step-and-hold servo controls, dynamic alignment, modulation–demodulation signal generation, and bench routine diagnostics. The properly existing non-zero friction of the air-cushioned interferometer with full DSP control allows the moving mirror to stop completely for step-scan data collection.

The Nexus 870's dynamic alignment keeps the interferometer in nearly perfect alignment during a scan and improves the line shape for high-resolution scans. Dynamic alignment actively compensates for any potential optical misalignment caused by ambient temperature changes or environmental vibration disturbances. This is achieved by monitoring the signal phases of two orthogonally located and one centrally located dc-coupled laser detectors at each mirror position (step). The dynamic alignment is active during the mirror presettling of each step. This ensures that the same phases between the three laser detectors are identical to the previous step. It becomes inactive when the moving mirror

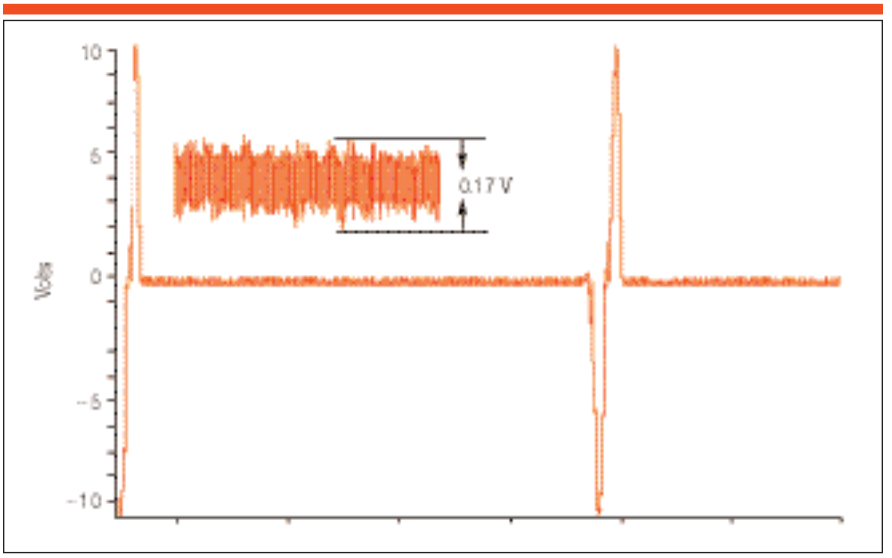

Figure 1. The mirror position accuracy of a Nexus 870 spectrometer was calculated from the measured peak-to-peak noise of the He-Ne laser signal: $d\delta \approx \pm 0.5(633/4\pi)(0.17/20) = \pm 0.2$ nm.

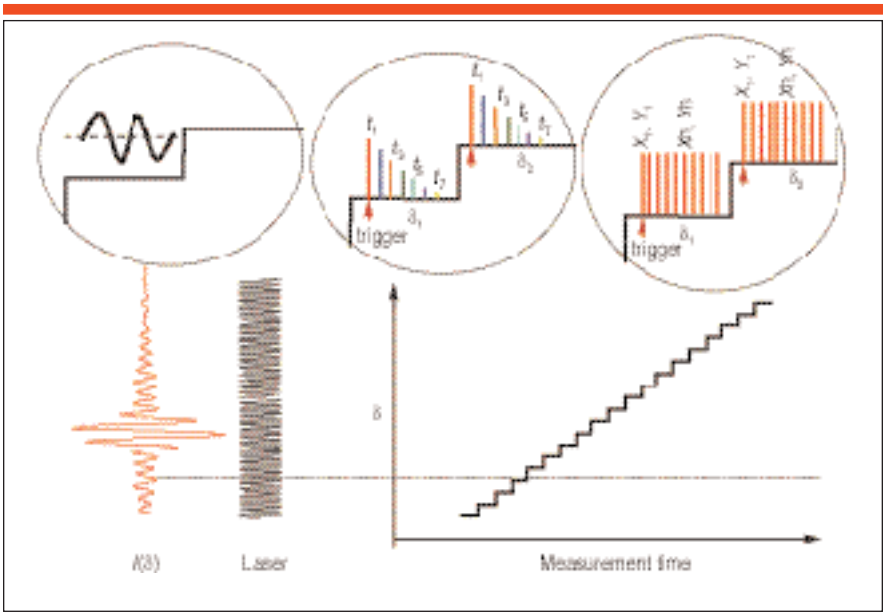

Figure 2. The data acquisition schemes for phase-, time-, and space-resolved step-scan FT-IR experiments (from left to right). Interferograms corresponding to each phase, time, and detector element are recorded as the mirror steps. Thus phase-, time-, and space-resolved spectra are obtained by fast Fourier transform.

comes to a complete stop for data collection.

The designs of the interferometer and the advanced DSP control algorithms make the Nexus 870 spectrometer nearly immune to ambient acoustic noises or vibrations. As shown in Figure 1, the mirror position accuracy of the Nexus 870 spectrometer (±0.2 nm) was calculated with the peak-to-peak noise of the laser signal that was measured when the instrument was placed on a regular laboratory table. The low peak-to-peak noise is a critical performance requirement to ensure all step-scan experiments have a high signal-to-noise ratio.

In addition, the open architecture design of step-scan experiment modules allows easy accommodation to new experiments. The high degree of integration also allows all FT-IR users to employ advanced step-scan techniques effectively without having to be instrumentation specialists.

STEP-SCAN FT-IR APPLICATIONS

Applications of step-scan FT-IR can be classified into three primary categories:

- Phase-resolved spectroscopy (PRS), or modulation experiments
- Time-resolved spectroscopy (TRS)
- Space-resolved spectroscopy (SRS), or array detector–based imaging.

Data-acquisition schemes for all three types of experiments are illustrated in Figure 2. At each mirror position, the data in Figure 2 were collected at 0° (in-phase) and 90° (quadrature) in step-scan PRS; at time intervals defined by the digitizer in TRS; or from all detector elements (pixels) in SRS. Interferograms corresponding to each phase, time, and detector element were constructed and phase-, time-, and space-resolved spectra were then computed by performing a fast Fourier transform on the interferogram data sets.

I. STEP-SCAN PRS — MODULATION EXPERIMENTS

Experiments in step-scan phase-resolved spectroscopy include three types of modulation techniques: amplitude modulation (IR intensity chopping), phase modulation (mirror dithering along retardation or path difference modulation), and sample modulation (sample under an external, usually sinusoidal, physical perturbation). In step-scan PRS experiments, the raw detector signal is demodulated by an external lock-in amplifier, a dedicated demodulator, or an internal DSP circuitry-based demodulator at the modulation frequency. The orthogonal outputs at phase angles 0° (in-phase) and 90° (quadrature) are then digitized simultaneously. Typical application examples of each modulation technique include the following.

Amplitude modulation — electroluminescence. In a step-scan amplitude modulation (AM) experiment, the intensity of the IR beam is modulated periodically either by chopping, synchronously varying the emission of a sample, or exciting the sample with synchronously varying sources. In all these cases, the energy hitting the detector varies at a constant frequency. The raw signal from the detector is first fed externally to a lock-in amplifier referencing the same modulation frequency. The maximized in-phase output signal is then digitized, recorded, and Fourier transformed to obtain a step-scan AM spectrum.

One typical application of step-scan AM is the characterization of electroluminescence of light-emitting devices in the mid-

and near-IR (NIR) region, with less restriction on the modulation frequency range. The Fourier frequency is eliminated in step-scan AM, and the modulated electrical or optical excitation with a desired single frequency is applied to the entire spectrum. This allows the device modulation to be tuned in a relatively wide range from ~10 to 100 kHz. In contrast, if a continuous scan mode is chosen, the device frequency should be at least a factor of 10 times higher than the fastest Fourier frequency: $F = 2v\delta$ in the spectral region of measurement spectrum, where v is mirror velocity (cm/s) and δ is IR frequency (cm^{-1}). This requirement restricts the range of electrical or optical modulation frequencies to be used to produce emission output, particularly in the lower modulation frequency range (~10 kHz).

Figure 3 shows a 0.5-cm^{-1} resolution step-scan electroluminescence spectrum from an iron-doped indium gallium arsenic phosphide (Fe:InGaAsP) light-emitting device (LED) (13). The emission power is on the order of 10 nW, which requires low duty cycles or low modulation frequency. Bands at high wavenumbers near 2825 cm^{-1} are attributed to intracenter transitions within the ^5D states of the Fe^{2+} ions substituted for indium and isotopic shift ($^{54}Fe/^{56}Fe$). Bands between 2600 and 2500 cm^{-1} are phonon sidebands that are associated with different acoustic, optic, and localized vibrational modes. The advantage of step-scan AM measurements on miniature and lowpower output is evident in the quality of the high-resolution spectrum.

Phase modulation — photoacoustic spectral depth profiling. In the Nexus 870 Vectra-Piezo step-scan interferometer, the phase modulation (PM) is produced by dithering the fixed mirror along retardation direction at a constant frequency. The DSP-controlled piezoelectric transducers actuate this dithering. The term "phase modulation" comes from the fact that the optical path difference modulation, or dithering, actually modulates the derivative, or phase, of the IR intensity. This design of the Vectro-Piezo step-scan interferometer allows PM frequencies and amplitudes to vary over the wide range typically needed for both NIR and mid-IR PM experiments. The design is also more flexible than systems that use ac-coupled interferometers. The reproducibility, stability, reliability, and flexibility of the Piezo-driven mirror is better than systems which rely on moving a much heavier moving mirror assembly for PM, due to easy DSP control of a relatively lighter fixed-mirror assembly.

One of the most advantageous applications of step-scan PM is photoacoustic spectral depth profiling (14). Photoacoustic spectroscopy (PAS) has gained much attention and popularity recently in chemical analysis because of a unique combination of features:

- Nondestructive, noncontact measurement
- Simple sample preparation
- Depth profiling (resolving) capability
- High signal saturation limit.

Photoacoustic signal generation includes absorption of modulated optical illumination (modulation frequency within an acoustic range) by the sample, thermal diffusion from within the sample to the adjacent medium (usually helium), and pressure oscillation of helium. The

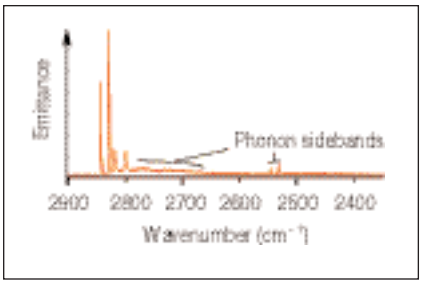

Figure 3. 0.5-cm^{-1} resolution step-scan electroluminescence spectrum of an iron-doped indium gallium arsenic phosphide (Fe:InGaAsP) LED. The emission power is on the order of 10 nW, which requires low duty cycles or low modulation frequency.

pressure wave (sound) is then detected using a very sensitive microphone. In PAS, a strong absorber across the spectrum such as carbon black, carbon black–filled materials (the content of carbon black must be more than 60%), or glassy carbon black is used to produce an energy profile of the instrument for intensity normalization of the sample PAS data. In recent experiments, the glassy carbon has proved to be an excellent surface phase reference material in depth profiling analysis (15).

When a photoacoustic sampling accessory (with a microphone built in as the detector) is coupled with a step-scan PM FT-IR, it becomes a very distinctive and powerful tool for obtaining depth-profiling information of heterogeneous or laminate samples. First, in a step-scan FT-IR PAS experiment, a uniform probing depth across the entire spectrum is achieved by using a constant PM on the fixed mirror. This provides an advantage over continuous scan FT-IR PAS, where the probing depth is wavenumber dependent. The DSP processors are used to perform the PM and demodulation required in photoacoustic experiments without the need of an external lock-in amplifier. The PM frequency determines the photoacoustic probing depth (inversely proportional to the square root of PM frequency) and the PM amplitude, which is expressed in terms of the He-Ne laser wavelength (λ_{HeNe}), defines the modulation efficiency and affects the energy profile over the entire spectrum.

Under a typical setting, the PM frequency of 100 Hz and the PM amplitude of 3.5 λ_{HeNe}, the probing depth (thermal diffusion length), μ, for most homogeneous organic polymers is 18 μm, ($\mu = 180/[f]^{1/2}$ {11}, where f is the modulation frequency and the unit for μ is micrometer) and the energy profile optimizes mid-IR spectral measurements. When heterogeneous– layered samples are involved, the actual probing depth can be as deep as 2 μ (twice the thermal diffusion length) if the overlayer is acting as an IR transparent window over the absorption region of the underneath layer (16). Thus by changing PM, one can obtain frequency-resolved depth profiling results.

Secondly, photoacoustic signal phase (ϕ) can be easily derived from the orthogonal in-phase (I) and quadrature (Q) spectra in a step-scan FT-IR PAS experiment by $\phi = \tan^{-1}(Q/I)$, which is not readily available from continuous scan PAS. The phase of a photoacoustic signal characteristically represents its spatial

origin. A photoacoustic signal from a deeper layer (part) will be detected later than those from a shallower layer (part). The relationship has been quantitatively elucidated in the photoacoustic phase theory for multilayer materials (17).

One of the important advantages of using photoacoustic signal phase in depth profiling is the enhancement of spatial resolution (as high as the submicrometer level, beyond the IR diffraction limit) within a given probing depth determined by modulation frequency and materials properties. Figure 4 illustrates the photoacoustic magnitude (top) and phase spectrum (bottom) of a three-layered sample, polymethyl methacrylate (PMMA) on polystyrene (PS) on 2-mm polypropylene (PP), collected at 200 Hz and 3.5 $\lambda_{He\text{-}Ne}$. Both of the top two layers are ≤0.5 μm thick. The phase spectrum clearly distinguishes characteristic bands from different layers by the phase angles; for example, the relative phase lags of 0.1°, 3°, and 18° correspond to distinctive bands of PMMA (1727 cm^{-1}, C=O stretch), PS (748 cm^{-1}, aromatic C–H deformation) and PP (1376 cm^{-1}, C–H deformation), respectively. In addition, the top two layers fit the phase difference model well for thermally thin and optically transparent layers (17). The thickness of the PMMA layer, d_{PMMA}, can then be determined by the phase difference model: $d_{PMMA} = \mu_{200\ Hz}\,\Delta\phi = 12.7(3 - 0.1)(\pi/180) = 0.6$ μm. This is very close to the actual thickness of about 0.5 μm. PAS clearly can discriminate submicrometer layers using the phase information. This detection capability is certainly beyond IR diffraction limits as seen in IR microscopic analysis.

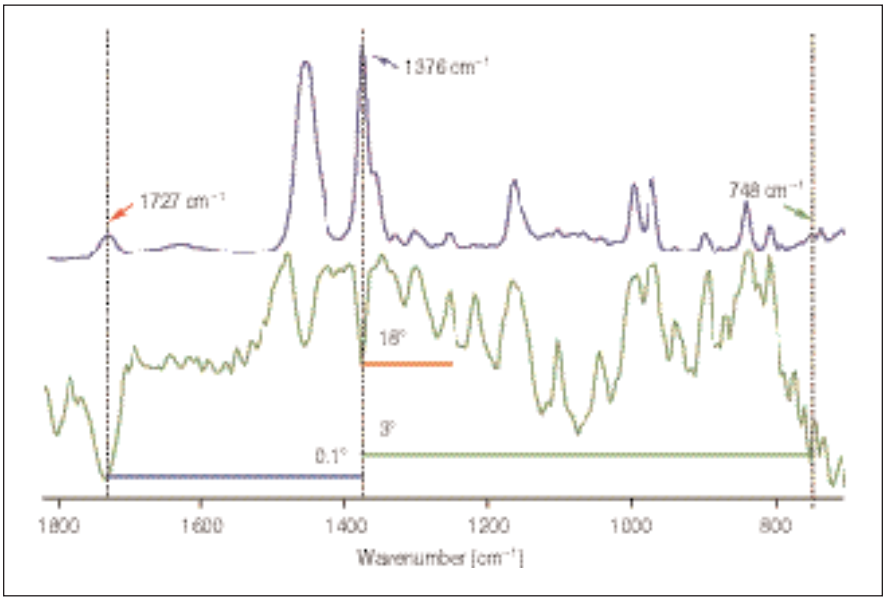

Figure 4. Photoacoustic magnitude (top) and phase spectrum (bottom) of a three-layered sample, ≤0.5-μm polymethyl methacrylate (PMMA) on ≤0.5-μm polystyrene (PS) on 2-mm polypropylene (PP), collected at 200 Hz and 3.5 $\lambda_{He\text{-}Ne}$. The characteristic bands of PMMA, PS, and PP are located at 1727 cm^{-1}, 748 cm^{-1}, and 1376 cm^{-1}, respectively.

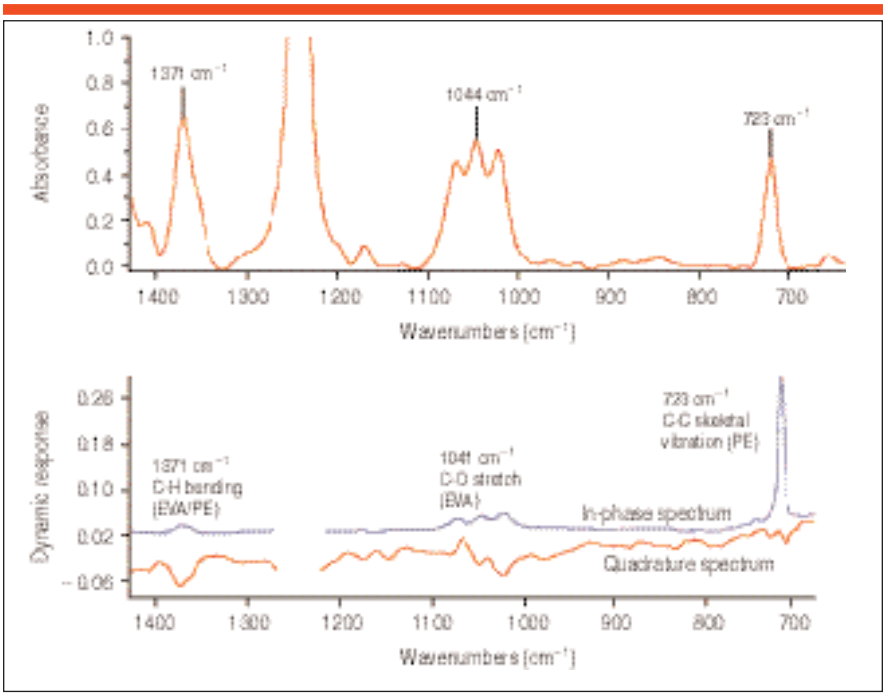

Figure 5. Absorbance (top), dynamic in-phase and quadrature spectra (bottom) of a polyethylene (PE)–ethylene-vinyl acetate (EVA) blend film composed of 7.6-μm PE on 29-μm EVA (9% vinyl acetate) on 4.6-μm methyl acrylate Sarun on 22-μm EVA (11% vinyl acetate), lower-density PE blend.

As reported and reviewed earlier, a few other depth profiling analysis approaches have been used in FT-IR PAS, such as time-resolved FT-IR PAS, generalized 2-D FT-IR PAS, and linearized FT-IR PAS (19–21). The frequency-resolved and phase-resolved FT-IR PAS are presently the most popular approaches in practical applications.

Sample modulation — polymer stretching. Because step-scan FT-IR decouples the time-dependent Fourier effect, it has been demonstrated to be the technical choice to obtain dynamic spectral information from samples under a repeatable–sinusoidal modulation of a physical parameter (14). These parameters can be of any physical quantity, such as mechanical strain, electric potential or temperature, and so forth. Usually, the frequency of sample modulation is small (~20 Hz), thus a faster carrier frequency, such as PM (~400 Hz), is simultaneously employed to increase the responsibility of sensitive mercury cadmium telluride (MCT) detectors and reduce or eliminate $1/f$ noise. Sample modulation is thus referred to as a *synchronous multiple modulation experiment* because it usually involves two or three modulations concurrently applied to the system.

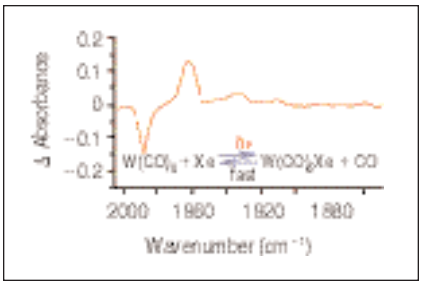

Figure 6. Spectral slice at 10 ns of photo-induced chemical reaction taken from a four-scan, 2-h step-scan TRS data collection.

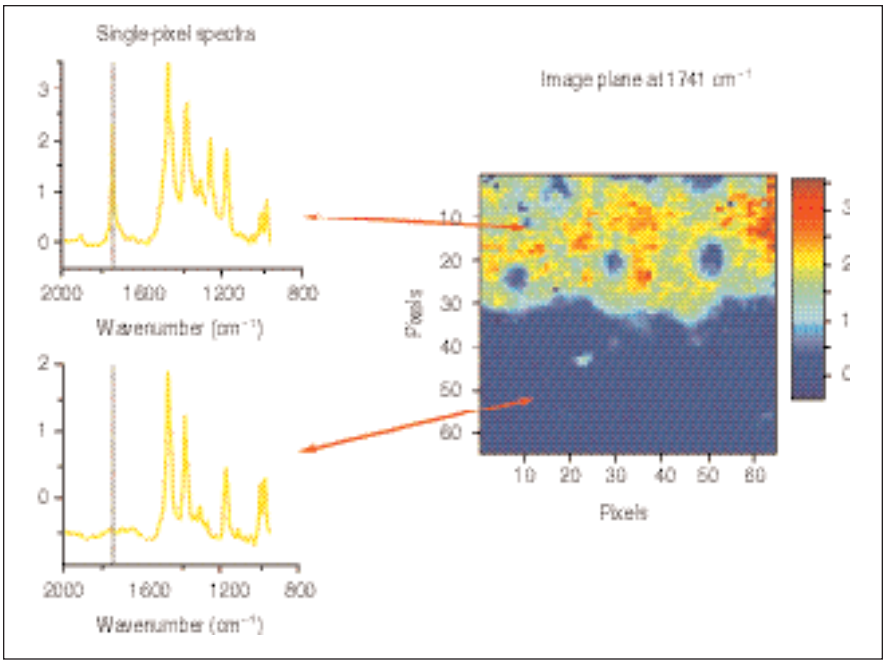

Figure 7. Spectral imaging plane at 1741 cm^{-1} (C = O stretching) and two single-pixel (60 μm × 60 μm) spectra extracted from the polypropylene and the organic sheet domains, respectively.

One of the typical applications of FT-IR sample modulation is the polymer stretching experiment. This experiment has been studied extensively in dynamic mechanical analysis (materials rheology). The purpose of applying FT-IR to this experiment is to determine the microscopic (molecular) basis for macroscopic (rheological or viscoelastic) properties. In particular, this refers to the degree of association in polymer blends, coherence of functional group motions within molecules, resolution of closely spaced bands, and quantitative correlation between macroscopic and microscopic phase delays.

In this experiment, the stretcher can be mounted directly on a base plate in the sample compartment, because the Vectra-Piezo interferometer is virtually immune to vibrations. The sample is mounted between the two jaws of the stretcher. One jaw is driven by a piezoelectric transducer to produce a sinusoidal mechanical strain at the frequency and amplitude set by the controller.

Initially, dynamic FT-IR polymer stretching experiments required two lock-in amplifiers (22, 23). One amplifier demodulated the raw signal of the PM and maximized the in-phase output, and the other demodulated the signal of the sample modulation. Modern step-scan FT-IR greatly simplifies this complicated experiment by using the circuitry of multiple DSPs (12). The DSPs may be perceived as internally built-in, digital lock-in amplifiers with large dynamic ranges. The open architecture design of the DSPs also allows easy accommodation to any other sample modulation experiment with different perturbations, such as electrochemical reactions (24) and liquid crystal dynamics (25).

In the polymer stretching experiment, an ideal elastic reference — a chopper (which can be built easily by mounting two small pieces of business cards to the two jaws of the stretcher, leaving a reasonably small gap in between. This gap can be adjusted to increase the modulation efficiency) is used to set the reference phases for each DSP demodulation, such that the in-phase responses of both the phase and sample modulations are maximized. This maximizes the elastic responses of the sample in the in-phase channel because the IR intensity varies simultaneously with the chopper.

Figure 5 shows the absorbance spectrum and dynamic in-phase and quadrature spectra of a polyethylene (PE)–ethylene-vinyl acetate copolymer (EVA) blend film. This film is composed of 7.6-μm PE on 29-μm EVA (9% vinyl acetate) on 4.6-μm methyl acrylate Sarun on 22- μm EVA (11% vinyl acetate), low-density PE blend. The data in Figure 5 were collected at a PM frequency of 400 Hz, amplitude of 3.5 $\lambda_{He\text{-}Ne}$ and a sample modulation frequency of 20 Hz. The sample was prestretched from 63.2 μm to 45 μm in thickness so that the intensity of bands of interest at 1371 cm^{-1} (EVA–PE), 1044 cm^{-1} (EVA), and 723 cm^{-1} (PE) were all less than 0.75 absorbance units, ensuring linearity of the dynamic measurement. The dynamic spectra show that the side chain bands at 1371 cm^{-1} (EVA–PE, C–H bending) and 1041 cm^{-1} (EVA, C–O stretching) have stronger quadrature contributions, indicating they are the major viscous component of the overall rheological properties. The very strong in-phase dynamic band at 723 cm^{-1} (PE, C–C skeletal vibration) demonstrates strong elastic contribution of the backbone (C–C) to the rheological properties of the blend material. However, the difference in rheological contributions from the pure PE layer and from the PE component of the blend layer can hardly be distinguished using the transmission-based stretching measurement. A more sophisticated attenuated total reflectance-based pressure–shearing modulation experiment, as described earlier (26), might be the preferred technical choice to discriminate between the subtle differences in dynamic responses.

Other data analysis approaches used in polymer stretching experiments include conventional 2-D–IR correlation (27) and phase and power (magnitude) spectral analysis (28). In addition, the dynamic polymer stretching experiment can be easily extended to study dynamic dichroic properties of polymeric materials by coupling the step-scan DSP-based stretcher setup with a photoelastic modulator.

II. STEP-SCAN TIME-RESOLVED SPECTROSCOPY

Step-scan time-resolved spectroscopy is well suited to obtaining spectral and kinetic information on fast, repeatable

chemical reactions or physical processes with time resolutions from microseconds to nanoseconds. In step-scan TRS, data are collected as an explicit function of time at each mirror position when both mirrors are stopped completely, as illustrated in Figure 2. This time profile is repeated and recorded at all mirror positions. After the experiment finishes, the data are sorted into individual interferograms that are then transformed into IR spectra at different times. The meaningful time resolution of step-scan TRS is determined by both the speed of the digitizer and the rise time of the detector, rather than by the scanning (stepping) speed.

Multiple triggers and coadditions at each mirror position, together with multiple scans, are often used to improve signal-to-noise ratio. The step-scan TRS spectrometer can be operated either in master operation mode (where the spectrometer triggers the excitation system of the sample) or slave mode (where the excitation system triggers the spectrometer). An external perturbation-induced reversible system can be readily studied by step-scan TRS. Irreversible systems can also be investigated by step-scan TRS if the process can be regenerated by moving a fresh sample into the beam for each mirror position (step) with a motorized stage or a stop-and-flow cell (29, 30), or a motorized stage (31).

The repeatable reactions or processes are often initiated with an external perturbation. External perturbations used in step-scan TRS vary in different application areas. The most common perturbations include

- Electric perturbation (32) — an electric pulse used in studying materials such as liquid crystals, polymer-dispersed liquid crystals, LEDs, or laser diodes
- Mechanical perturbation (33) — mechanical strain or pressure used in polymer stretching and shearing experiments; rapid mixing used in stop-and-flow kinetics
- Optical perturbation (34–36) — a laser or flashlamp pulse used in photochemical studies (excited states of metal complexes and photochemical reactions in condensed or gaseous phase) and biophysics (photocycles of bacteriorhodopsin)
- Thermal perturbation (37) — temperature jumps used in biophysics studies (protein conformational changes).

An example application of step-scan TRS is the study of the reversible chemical reaction (36) illustrated in Figure 6. $W(CO)_5(Xe)$ was generated in situ by a 308-nm laser pulse in a supercritical Xe and CO solution. The lifetime of this reaction is ~100 ns, thus the spectra can only be measured by FT-IR in step-scan mode. The difference spectrum shown in Figure 6 is a 10-ns time slice of the TRS spectra from a four-scan data collection, indicating a decrease in concentration of the reactant.

III. STEP-SCAN SPACE-RESOLVED SPECTROSCOPY — IMAGING

In a step-scan space-resolved spectroscopy (SRS) imaging system, a DC-coupled focal plane array IR camera with MCT or InSb arrays is used. At each interferometer mirror position, a trigger

signal is sent to the camera to collect a series of interferometric frames from all pixels. The image frames are then averaged for each retardation position (38). Multiple scans can also be used to improve the overall signal-to-noise ratio. The interferometric image data are then resorted or resolved by detector element (pixel) location, and then Fourier transformed. In this manner, the space-resolved spectra or spectral images at different wavenumbers can be generated. A new imaging system, ImageMax (Thermo Nicolet), combines the latest technologies for the interferometer, microscope, and imaging into a single integrated system. The ImageMax, based on a Nexus 870 step-scan spectrometer, is designed for both routine and advanced imaging data collection, processing, and quantitation.

The ImageMax system can be used to visualize the spatial distribution of distinct chemical species in a variety of systems. Massive imaging data sets can be recorded with the system in a fraction of the time required by a traditional mapping experiment. The ImageMax accommodates both transmission and reflectance illumination modes for imaging in microscopic mode (400 μm × 400 μm) as well as for large area samples (4 mm × 4 mm), without having to relocate the array detector. The most popular MCT focal-plane array detector has 64 × 64 pixels with a long wavelength cutoff at approximately 900 cm^{-1}.

The average spatial resolution for mid-IR can be as high as 5 μm for micro sampling and 50 μm for macro sampling. The versatile imaging data acquisition and analysis software packages with univariate and multivariate approaches, as well as statistical representations, offer the power and convenience of sophisticated quantitative imaging analysis. Wide applications of this powerful technique to the analysis of heterogeneous samples have been found in fields of biomedical, life, and materials sciences (39–41), as well as in many other potential fields such as pharmaceutical characterizations.

Figure 7 shows the spectral imaging plane at 1741 cm^{-1} (C=O stretching) and two single-pixel (60 μm × 60 μm) spectra extracted from the polypropylene and the organic sheet domains respectively. The data were collected in the macro reflectance mode with a 64 × 64 MCT array detector. The spatial distribution of the organic sheet (with C=O) is highlighted in the image. The spectra at different spatial locations or images at different wavenumbers can be easily extracted or constructed by using the imaging software. Other advanced quantitative and statistic imaging data analysis tools such as principal component analysis, partial least squares regression, and fuzzy C-means clustering and factor analysis are also available in the software package.

SUMMARY AND FUTURE TRENDS

From an old concept to modern instrument redevelopment, step-scan FT-IR has been gaining popularity among researchers and analysts during the past decade. The technology advancement has featured the extensive implementation of multiple digital processors in modern step-scan FT-IR spectrometers. The air-

cushioned graphite vectra-piezo interferometer design has improved the stability, reliability, and performance of the modern step-scan FT-IR spectrometer and widened FT-IR applications to many areas. Broad applications of step-scan FT-IR in studying phase-, time-, and space-dependent phenomena have been demonstrated with typical examples. These include electroluminescence measurement of low-powered light-emitting devices; depth profiling of submicrometer-thick multilayered polymer films; dynamic rheological characterization of polymer blends; fast chemical reactions on the nanosecond time scale; rapid and massive imaging data acquisition, and analysis of heterogeneous samples. The technological advancement in fast electronics, digital signal processing, alternative IR radiation sources, and sensitive and quantitative detectors will continuously improve the performance and widen the applications of modern step-scan FT-IR in years to come.

ACKNOWLEDGEMENT

The author would like to acknowledge Mike George of the University of Nottingham (United Kingdom) for providing the ns TRS spectrum, and Neil Lewis and Linda Kidder of Spectral Dimensions (Olney, MD) for collecting the imaging data.

REFERENCES

(1) J. Connes and P. Connes, *J. Opt. Soc. Am.* **56,** 896 (1966).
(2) C. Manning and R.A. Palmer, *Rev. Sci. Instrum.* **62,** 1219 (1991).
(3) A. Simon, *Sixth International Conference on Fourier Transform Spectroscopy*, August, 1987, Vienna, Austria.
(4) R.A. Crocombe, R. Curbelo, J. Leonardi, and D.B. Johnson, *SPIE Proc.* **1575,** 189 (1991).
(5) V.G. Gregoriou, M. Daun, M.W. Schauer, J.L. Chao, and R.A. Palmer, *Appl. Spectrosc.* **47,** 1311 (1993).
(6) M.J. Smith, C.J. Manning, R.A. Palmer, and J.L. Chao, *Appl. Spectrosc.* **42,** 546 (1988).
(7) R.A. Palmer, J.L. Chao, R.M. Dittmar, V.G. Gregoriou, and S.E. Plunkett, *Appl. Spectrosc.* **47,** 1297 (1993).
(8) T. Nakano, T. Yokoyama, and H. Toriumi, *Appl. Spectrosc.* **47,** 1354 (1993).
(9) T.J. Johnson, A. Simon, J.M. Weil, and G.W. Harris, *Appl. Spectrosc.* **47,** 1376 (1993).
(10) C.J. Manning and P.R. Griffiths, *Appl. Spectrosc.* **47,** 1345 (1993).
(11) D.L. Drapcho, R. Curbelo, E.Y. Jiang, R.A. Crocombe, and W.J. McCarthy, *Appl. Spectrosc.* **51,** 453 (1997).
(12) P.Y. Chen and M.J. Smith, *Advanced Experiments on Nicolet Step-scan Spectrometers*, Thermo Nicolet (Madison, WI) Applications Booklet (1999).
(13) R. Hapanowicz, *Laser Focus World,* **32**(7), 65–74 (1996).
(14) R.A. Palmer, *Spectroscopy* **8**(2), 26 (1993).
(15) R. Jones, S. Bajic, and J. McClelland, paper 1261 presented at the 1999 Pittsburgh Conference (Orlando, FL).
(16) R.A. Palmer and R.M. Dittmar, *Thin Solid Films,* Section A **223,** 31 (1993).
(17) E.Y. Jiang, R.A. Palmer, and J.L. Chao, *J. Appl. Phys.* **78,** 460 (1995).
(18) E.Y. Jiang, R.A. Palmer, N.E. Barr, and N. Morosoff, *Appl. Spectrosc.* **51,** 1238 (1997).
(19) E.Y. Jiang, W.J. McCarthy, D.L. Drapcho,

and R.A. Crocombe, *Appl. Spectrosc.* **51,** 1736 (1997).
(20) E.Y. Jiang, W.J. McCarthy, and D.L. Drapcho, *Spectroscopy* **13**(2), 21–40 (1998).
(21) E.Y. Jiang and M.J. Smith, "Application Note AN-01127" (Thermo Nicolet, Madison, WI, 2001).
(22) B.O. Budevska, C.J. Manning, P. Griffiths, and R.T. Roginski, *Appl. Spectrosc.* **47,** 1843 (1993).
(23) V.G. Gregoriou, I. Noda, A.E. Dowrey, C. Marcott, J.L. Chao, and R.A. Palmer, *J. Polymer Science* **31,** 1769 (1993).
(24) C.P. Pharr and P. Griffiths, *Appl. Spectrosc.* **50,** 1360 (1996).
(25) V.G. Gregoriou, J.L. Chao, H. Toriumi, and R.A. Palmer, *Chem. Phys. Letter* **179,** 491 (1991)
(26) C. Marcott, G.M. Story, I. Noda, A. Bibby, and C.J. Manning, in *Fourier Transform Spectroscopy, Proceedings of the 11th International Conference on Fourier Transform Spectroscopy*, Ed. J.A. deHaseth, AIP Proceedings 430, 379 (American Institute of Physics, College Park, MD, 1998).
(27) I. Noda, *Appl. Spectrosc.* **44,** 550 (1990).
(28) B.O. Budevska, C.J. Manning, and P.R. Griffiths, *Appl. Spectrosc.* **48,** 1556 (1994).
(29) S.E. Bromberg, H. Yang, M.C. Asplund, T. Lian, B.K. McNamara, K.T. Kotz, J.S. Yeston, M.Wilkens, H. Frei, R.G. Bergman, and C.B. Harris, *Science* **278,** 260 (1997).
(30) E. Kauffmann, H. Frei, and R.A. Mathies, *Chem. Phys. Lett.* **266,** 554 (1997).
(31) R. Rammelsberg, S. Boulas, H. Chorongiewski, and K. Gerwert, *Vibrational Spectrosc.* **19,** 143–149 (1999).
(32) T. Nakano, T. Yokoyama, and H. Toriumi, *Appl. Spectrosc.* **47**(9), 1354 (1993).
(33) H. Wang, R.A. Palmer, and C.J. Manning, *Appl. Spectrosc.* **51**(8), 1245 (1997).
(34) S.E. Plunkett, J.L. Chao, T.J. Tague, and R.A. Plamer, *Appl. Spectrosc.* **49,** 702 (1995).
(35) M. Shim, S.V. Shilov, M.S. Braiman, and P. Guyot-Sionnest, *J. Phys. Chem.* **B104,** 1494–1496 (2000).
(36) X.Z. Sun, S.M. Nikiforov, and M.W. George, in *Proceedings of the 12th International Conference on Fourier Transform Spectroscopy*, 239 (Waseda University Press, Tokyo, 1999).
(37) S. Williams, T.P. Causgrove, R. Gilmanshin, K.S. Fang, R.H. Callender, W.H. Woodruff, and B.R. Dyer, *Biochemistry* **35,** 691–697 (1996).
(38) E. Neil Lewis, P.J. Treado, R.C. Reeder, G.M. Story, A.E. Dowrey, C. Marcott, and I.W. Levin, *Anal. Chem.* **67,** 3377 (1995).
(39) P.J. Treado, I.W. Levin, and E.N Lewis, *Appl. Spectrosc.* **48,** 5 (1994).
(40) L.H. Kidder, V.F. Kalasinsky, J.L. Luke, I.W. Levin, and E.N Lewis, *Nature Medicine* **3**(2), 235 (1997).
(41) L.H Kidder, P. Colarusso, S.A. Stewart, I.W. Levin, N.M. Appel, D.S. Lester, P.G. Pentchev, and E.N. Lewis, *Journ. Biomedical Optics* **41**(1), 7–13 (1999).

Eric Y. Jiang *is research products manager at Thermo Nicolet* (Madison, WI). *He obtained his Ph.D. in Physical Chemistry from Duke University (Durham, NC) under the guidance of Richard A. Palmer. His research interests cover a broad range of advanced vibrational spectroscopy, including photoacoustic spectroscopy, time-resolved spectroscopy, polarization modulation spectroscopy, applications of 2-D-correlation spectroscopy, spectroscopic imaging, and so forth. He may be contacted by e-mail at author@thermonicolet.com.* ◆